Endoplasmic Reticulum Glucosidase II Is Inhibited by Its End Products

Eran Bosis,[‡] Esther Nachliel,[‡] Tamar Cohen,[‡] Yoichi Takeda,[§] Yukishige Ito,[§] Shoshana Bar-Nun,*[,‡] and Menachem Gutman*[,‡]

Department of Biochemistry, George S. Wise Faculty of Life Sciences, Tel Aviv University, Tel Aviv 69978, Israel, and RIKEN (The Institute of Physical and Chemical Research), 2-1 Hirosawa, Wako, Saitama 351-0198, Japan

Received August 15, 2008

ABSTRACT: The calnexin/calreticulin cycle is a quality control system responsible for promoting the folding of newly synthesized glycoproteins entering the endoplasmic reticulum (ER). The association of calnexin and calreticulin with the glycoproteins is regulated by ER glucosidase II, which hydrolyzes $Glc_2Man_XGlcNAc_2$ glycans to $Glc_1Man_XGlcNAc_2$ and further to $Glc_0Man_XGlcNAc_2$ (*X* represents any number between 5 and 9). To gain new insights into the reaction mechanism of glucosidase II, we developed a kinetic model that describes the interactions between glucosidase II, calnexin/calreticulin, and the glycans. Our model accurately reconstructed the hydrolysis of glycans with nine mannose residues and glycans with seven mannose residues, as measured by Totani et al. [Totani, K., Ihara, Y., Matsuo, I., and Ito, Y. (2006) *J. Biol. Chem. 281*, 31502−31508]. Intriguingly, our model predicted that glucosidase II was inhibited by its nonglucosylated end products, where the inhibitory effect of $Glc_0Man_7GlcNAc_2$ was much stronger than that of $Glc_0Man_9GlcNAc_2$. These predictions were confirmed experimentally. Moreover, our model suggested that glycans with a different number of mannose residues can be equivalent substrates of glucosidase II, in contrast to what had been previously thought. We discuss the possibility that nonglucosylated glycans, existing in the ER, might regulate the entry of newly synthesized glycoproteins into the calnexin/calreticulin cycle. Our model also shows that glucosidase II does not interact with monoglucosylated glycans while they are bound to calnexin or calreticulin.

The secretory pathway is responsible for synthesis, maturation, and transport of proteins destined to the cell surface as well as to cellular organelles along this pathway. Proteins of the secretory pathway are synthesized by ribosomes bound to the cytosolic side of the endoplasmic reticulum (ER),[1] and the nascent chains are translocated to the ER through the Sec61 translocation channel (*1*). As soon as the proteins enter the ER, they start to fold into their final functional conformations. An array of chaperones assists the folding of the proteins, and a quality control system ensures that only correctly folded proteins would leave the ER (*2*). By preventing the premature exit of folding intermediates, the quality control system extends the exposure of substrates to the folding machinery in the ER and thereby enhances the probability of correct maturation.

Most of the secretory pathway proteins are modified within the ER lumen by the covalent binding of one or more glycans, composed of three glucose, nine mannose, and two *N*-acetylglucosamine residues ($Glc_3Man_9GlcNAc_2$) (Scheme 1) (*2*). The glycans are covalently linked to an asparagine residue in the consensus sequence Asn-X-Ser/Thr by the oligosaccharyltransferase complex located near the translocation channel. Immediately after the binding of the core glycan to the protein, the outer glucose residue is removed by glucosidase I (Scheme 1). The second glucose residue is then removed by glucosidase II, generating a monoglucosylated glycan that is recognized by either calnexin or calreticulin. These two homologous ER-resident chaperones have a single binding site for monoglucosylated glycans with a micromolar affinity (*3*−*5*). They also seem to recognize

Scheme 1: (A) Structure of the Core N-Linked Glycan[a] and (B) Processing of the N-Linked Glycan in the Calnexin/Calreticulin Cycle[b]

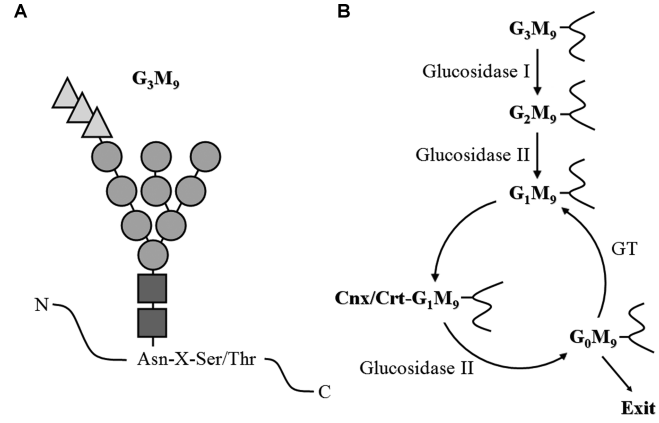

[a] D-glucose, D-mannose, and *N*-acetylglucosamine residues are represented by triangles, circles, and rectangles, respectively. [b] Abbreviations: Cnx, calnexin; Crt, calreticulin; GT, UDP-glucose:glycoprotein glucosyltransferase.

* Corresponding authors. S.B.-N.: tel, +972-3-6408984; fax, +972-3-6406834; e-mail, shoshbn@tauex.tau.ac.il. M.G.: tel/fax, +972-3-6409875; e-mail, me@hemi.tau.ac.il.

[‡] Tel Aviv University.

[§] RIKEN.

[1] Abbreviations: ER, endoplasmic reticulum; GT, UDP-glucose: glycoprotein glucosyltransferase; Cnx/Crt, calnexin/calreticulin; ERAD, ER-associated protein degradation; MTX, methotrexate; G_2M_X, $Glc_2Man_XGlcNAc_2$; G_1M_X, $Glc_1Man_XGlcNAc_2$; G_0M_X, $Glc_0Man_XGlcNAc_2$.

10.1021/bi801545d CCC: $40.75
Published on Web 09/20/2008

nonnative glycoproteins through a polypeptide-binding site specific for nonnative conformers (*6*). Together with the thiol−disulfide oxidoreductase ERp57, calnexin and calreticulin assist in the folding of the glycoprotein. It is currently accepted that the removal of the remaining single glucose residue by glucosidase II results in the release of the nonglucosylated glycoprotein substrate from calnexin and calreticulin (Scheme 1). At this stage, if the glycoprotein is correctly folded, it can proceed to the ER exit site from where it is transported by vesicles to its ultimate destination. Otherwise, the aberrant glycoprotein is reglucosylated to the monoglucosylated state by UDP-glucose:glycoprotein glucosyltransferase (GT) (*7*), enabling calnexin and calreticulin to reassociate with the glycoprotein. In this way, calnexin and calreticulin can cycle on and off the glycoprotein until it is properly folded. A terminally misfolded glycoprotein, which is retained in the calnexin/calreticulin cycle for a long period, will eventually be trimmed by slow-acting mannosidases located in the ER (*8*). Trimming of mannose residues was shown to reduce the activity of both glucosidase II and GT toward the glycoprotein (*9, 10*). Mannose trimming is thought to irreversibly release the glycoprotein from the calnexin/calreticulin cycle and target it for ER-associated degradation (ERAD) (*11*−*14*).

To gain new insights into the reaction mechanism of glucosidase II, we developed a kinetic model that describes the interactions between glucosidase II, calnexin/calreticulin, and the N-linked glycans. Our model was based on the experimental results of Totani et al. (*15*), who studied the substrate specificity of glucosidase II using synthetic oligosaccharides identical in their structure to the native N-linked glycans. The model consisted of six reversible and irreversible reactions, which were translated into a set of coupled nonlinear ordinary differential equations. We employed the Genetic Algorithm to search for the rate constants of the reactions.

Our model accurately reconstructed the hydrolysis of the M_9 and M_7 glycans, two substrates of glucosidase II, which differed in their reactivities. Furthermore, it predicted that glucosidase II is inhibited by its nonglucosylated end products, G_0M_9 and G_0M_7, and that the inhibitory effect of G_0M_7 is much stronger than that of G_0M_9. These predictions were later confirmed experimentally. We suggest that the lower reactivity of the M_7 glycans, compared to that of the M_9 glycans, does not result from lower specificity of glucosidase II to these glycans but from the inhibition of the catalysis by the accumulation of the more potent inhibitor, G_0M_7. Thus, glycans with a different number of mannose residues can be, at least in some cases, equivalent substrates of glucosidase II. We also showed that glucosidase II does not interact with the monoglucosylated glycans while they are bound to calnexin/calreticulin, suggesting that calnexin and calreticulin dissociate from their substrate spontaneously, i.e., without the involvement of glucosidase II, while the latter prevents their reassociation.

EXPERIMENTAL PROCEDURES

Model System. The current model is composed of six reactions, the first five deal with the interactions between glucosidase II and the glycan and the last one handles the interaction of calnexin/calreticulin with the monoglucosylated glycan. The sequence of events is given in Scheme 2. The model was converted into a set of coupled nonlinear ordinary differential equations using the standard chemical−kinetic formalism, according to which the velocity of the reaction is the product of the rate constant of the reaction multiplied by the concentrations of the reactants (*16*). The laborious task of converting the reactions into the differential equations was done automatically using a home-written program, the ODEBuilder, which is available with its source code upon request.

Scheme 2: Reaction Mechanism of Glucosidase II[a]

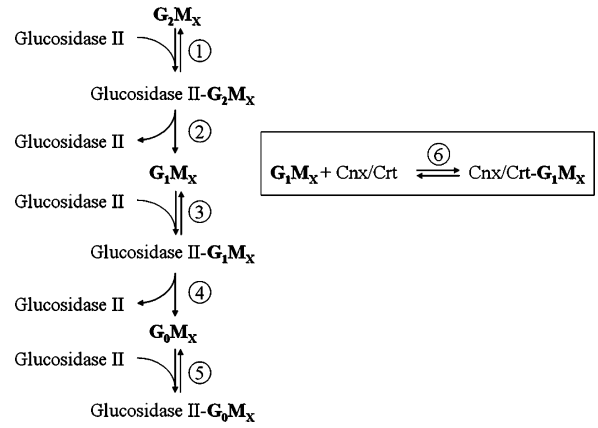

[a] The reaction mechanism of glucosidase II is composed of three reversible reactions (1, 3, and 5) and two irreversible catalytic reactions (2 and 4). Reaction 6 describes the reversible interaction of calnexin/calreticulin (Cnx/Crt) with G_1M_X. *X* represents any number between 5 and 9.

The coupled nonlinear ordinary differential equations corresponding with the reactions are

$$d[GII{-}G_2M_X]/dt = k_1[GII][G_2M_X] - k_{-1}[GII{-}G_2M_X] - k_2[GII{-}G_2M_X] \quad (1)$$

$$d[G_1M_X]/dt = k_2[GII{-}G_2M_X] - k_3[GII][G_1M_X] + k_{-3}[GII{-}G_1M_X] - k_6[Crt][G_1M_X] + k_{-6}[Crt{-}G_1M_X] \quad (2)$$

$$d[GII{-}G_1M_X]/dt = k_3[GII][G_1M_X] - k_{-3}[GII{-}G_1M_X] - k_4[GII{-}G_1M_X] \quad (3)$$

$$d[G_0M_X]/dt = k_4[GII{-}G_1M_X] - k_5[GII][G_0M_X] + k_{-5}[GII{-}G_0M_X] \quad (4)$$

$$d[GII{-}G_0M_X]/dt = k_5[GII{-}G_0M_X] - k_5[GII{-}G_0M_X] \quad (5)$$

$$d[Crt{-}G_1M_X]/dt = k_6[Crt][G_1M_X] - k_{-6}[Crt{-}G_1M_X] \quad (6)$$

The equations comply with the detailed balance principle and the law of conservation of mass. The current concentrations of the reactants are

$$[GII]_t = [GII]_0 - [GII{-}G_2M_X]_t - [GII{-}G_1M_X]_t - [GII{-}G_0M_X]_t$$

$$[G_2M_X]_t = [G_2M_X]_0 - [GII{-}G_2M_X]_t - [G_1M_X]_t - [GII{-}G_1M_X]_t - [G_0M_X]_t - [GII{-}G_0M_X]_t - [Crt{-}G_1M_X]_t$$

$$[Crt]_t = [Crt]_0 - [Crt{-}G_1M_X]_t$$

The experimental protocol, which we simulated in this study, was the one reported by Totani et al. (*15*). In brief, the reaction was initiated by the mixing of 50−400 μM

Table 1: Parameters Used for Reconstruction of the Reaction of Glucosidase II with M_9 Glycans

parameter	search range	result range: M_9 glycans	result range: M_9 glycans with Crt	units
k_1	1−1E9	1.5E4−1E9	1.6E4−1E9	M^{-1} s^{-1}
k_2	1E-3−1E6	1.79−311.05	1.63−319.9	s^{-1}
k_3	1−1E9	5.2E3−9.7E8	5.4E3−9.9E8	M^{-1} s^{-1}
k_4	1E-3−1E6	0.31−0.37	0.31−0.34	s^{-1}
k_5	1−1E9	1.5E2−5.5E8	2.8E2−9.5E8	M^{-1} s^{-1}
k_6	1−1E6		3.3E3−5.1E3	M^{-1} s^{-1}
K_{d1}	1E-9−1	1E-9−5.2E-3	1E-9−5.7E-3	M
K_{d3}	1E-9−1	1.1E-9−7.9E-5	1E-9−6.6E-5	M
K_{d5}	1E-9−1	1.3E-5−2.6E-5	1.5E-5−2.3E-5	M
K_{d6}			0.192E-6 (input)	M
α	0.5−1.0		0.69−0.71	

chemically synthesized glycan−methotrexate (MTX) conjugates with 0.56 milliunit of soluble rat liver glucosidase II (0.19 unit/mg of protein) in a total volume of 100 μL at 37 °C. Enzyme concentration was 200 nM, based on the molar weight of glucosidase II (150 kDa) (*17*). In some cases, the glucose trimming reactions were performed in the presence of calreticulin (25−75 μM). At given intervals, within a time window of 5−90 min, a small fraction of the reaction mixture was removed and heated at 100 °C to stop the enzymatic reaction. The percentage of glucose trimming in each reaction was analyzed by high-performance liquid chromatography (HPLC). The glycan−MTX conjugates were detected by measuring the absorption of MTX at 304 nm.

Simulation Procedure. The six coupled nonlinear ordinary differential equations were subjected to numeric integration, using the Runge−Kutta methods as embedded in the Matlab program (the ODE23S routine) (*18*). To fit the experimental results, the initial concentrations of the reactants were set according to the experimental protocol. The equations were propagated in time, and the concentrations of the intermediates and the final products were saved as vectors. The percentage of the various states of the glycan was calculated in the following way:

$$\%\,(G_2M_X) = 100([G_2M_X]_0 - [G_1M_X]_t - [GII{-}G_1M_X]_t - [G_0M_X]_t - [GII{-}G_0M_X]_t - [Crt{-}G_1M_X]_t)/([G_2M_X]_0)$$

$$\%\,(G_1M_X) = 100([G_1M_X]_t + [GII{-}G_1M_X]_t + [Crt{-}G_1M_X]_t)/([G_2M_X]_0)$$

$$\%\,(G_0M_X) = 100([G_0M_X]_t + [GII{-}G_0M_X]_t)/([G_2M_X]_0)$$

Evaluation of the Rate Constants. Reconstruction of the experimental observations would be possible only if the model is supplied with the appropriate rate constants. For this reason, our main task was to search for these values by treating the rate constants as adjustable parameters. The boundaries of the adjustable parameters are summarized in Tables 1 and 2. For the bimolecular reactions (k_1, k_3, and k_5), where the enzyme forms a complex with the glycan, we set the upper limit to 10^9 M^{-1} s^{-1}, which is the estimated value of the rate of encounter between the reactants, as calculated according to the Debye−Smoluchowski equation (*19*). In accordance with the notion that the number of glucose residues may affect the association of the enzyme with the glycan, the values of the bimolecular reactions were allowed to vary within 2 orders of magnitude. The reverse reactions (k_{-1}, k_{-3}, and k_{-5}) were set according to the dissociation constants of the complexes (K_{d1}, K_{d3}, and K_{d5}, respectively). To address differences in the stability of the enzyme−substrate complexes (*20*−*22*), K_{d1} and K_{d3} were allowed to vary within 2 orders of magnitude. No restrictions were imposed on K_{d5}. The upper limit of the irreversible catalytic constants (k_2 and k_4) was allowed to be 10^6 s^{-1}, much faster than the observed rate of catalysis. The values of k_2 and k_4 were allowed to vary within 3 orders of magnitude. The parameters dealing with calreticulin were set as follows: for the reaction of calreticulin with G_1M_9, the upper limit for the search was set to 10^6 M^{-1} s^{-1}, based on the measurements of Patil et al. (*3*), who found that the second-order rate constant of the reaction of calreticulin with G_1M_9 was several orders of magnitude slower than that of diffusion-controlled processes. The dissociation constant of the calreticulin−G_1M_X complex (K_{d6}) was set in the following way: the experimental value of the calreticulin−G_1M_9 complex (0.192 μM) (*4*) was accepted and used without any changes; in the simulations with G_1M_7, we let the Genetic Algorithm to search for it in the range between 0.4 μM (the experimental value of G_1M_{8B}) and 0.5 μM (the experimental value of the tetrasaccharide G_1M_3) (*23, 24*). An additional adjustable parameter, α, was included in the analysis to denote the active fraction of the purified calreticulin.

Table 2: Parameters Used for Reconstruction of the Reaction with M_7 Glycans

parameter	search range	result range	units
k_1	1−1E9	9.8E3−7.1E6	M^{-1} s^{-1}
k_2	1E-3−1E6	0.35−285	s^{-1}
k_3	1−1E9	4E3−3.8E6	M^{-1} s^{-1}
k_4	1E-3−1E6	0.2−0.3	s^{-1}
k_5	1−1E9	2.8E3−1.1E6	M^{-1} s^{-1}
k_6	1−1E6	1.8E3−1E6	M^{-1} s^{-1}
K_{d1}	1E-9−1	1E-9−2.3E-3	M
K_{d3}	1E-9−1	5.9E-9−6.5E-5	M
K_{d5}	1E-9−1	1.3E-9−4.9E-7	M
K_{d6}	0.4E-6−0.5E-6	0.4E-6−0.5E-6	M
α	0.5−1.0	0.62−0.69	

Fitness Function. The system reconstructed two sets of experiments: the effect of G_1M_X concentration on initial velocity of the catalytic reaction and the kinetics of the hydrolysis of G_2M_X to G_1M_X and G_0M_X. The fitness function, describing the level of agreement between the experimental signals and the simulated lines, is the sum of the squares of the distances of the simulated values from the borders of the experimental values. The data points, depicting the initial velocity of the catalytic reaction of glucosidase II, originally given in micromoles per hour per milligram, were multiplied by the mass of the enzyme (3×10^{-3} mg), and the outcome was divided by the volume of the reaction (10^{-4} L) and by 12 (for the time), to obtain the yield, in micromolar units, after 5 min. The borders of the experimental values were determined according to mean ± standard deviations as reported by Totani et al. (*15*). Any data point that fell within the borders of the experimental signal had no effect on the fitness value. To match the contribution of the two sets of experiments, correction factors were introduced rendering all deviations equal in determination of the final value of the fitness function.

Genetic Algorithm. The optimization of the fitness function was performed using the Genetic Algorithm Optimization Toolbox of Matlab (*25*). We used the default parameters of the toolbox as described previously (*16, 26*). Each run of the Genetic Algorithm lasted for 1000 generations.

Expanding the Model To Predict the Effect of G_0M_7. To predict the effect of G_0M_7 on the entry of newly synthesized glycoproteins into the calnexin/calreticulin cycle, we expanded our model to include a reversible reaction between glucosidase II and G_0M_7. The differential equation corresponding with this reaction is

$$d[GII{-}G_0M_7]/dt = k_7[GII][G_0M_7] - k_{-7}[GII{-}G_0M_7] \quad (7)$$

The current concentration of glucosidase II was changed accordingly:

$$[GII]_t = [GII]_0 - [GII{-}G_2M_X]_t - [GII{-}G_1M_X]_t - [GII{-}G_0M_X]_t - [GII{-}G_0M_7]_t$$

Glucosidase II Inhibition Assay. Reaction mixtures contained, in a total volume of 20 μL, 50 μM G_2M_9, 0.14 microunit of soluble rat liver glucosidase II (0.08 milliunit/mg of protein) (whose activity was measured using *p*-nitrophenyl α-D-glucopyranoside as a substrate (*17*), with one unit of enzymatic activity defined as the amount that releases 1 μmol/min *p*-nitrophenol at 37 °C), 1 mM deoxymannojirimycin, inhibitors (0.5−500 μM), 0.05% Triton X-100, 1 mM $CaCl_2$, and 10 mM Hepes (pH 7.4). Glucosidase II was preincubated with designated concentrations of G_0M_9, G_0M_{8B}, G_0M_{8C}, or G_0M_7. After 30 min at 37 °C, substrate was added and incubated further for 10 min at 37 °C. After the reactions were stopped by heating at 100 °C for 1 min, the mixtures were analyzed by HPLC under the following conditions: TSK-GEL Amide-80 column (4.6 mm i.d. × 25 cm), mobile phase CH_3CN/3% AcOH−Et_3N (pH 7.3), linear gradient from 65:35 to 50:50 in 50 min, and flow rate 1.0 mL/min at 40 °C. All assays were conducted in triplicate. The glycan−MTX conjugates were detected by measuring absorption at 304 nm.

RESULTS

Description of the Model. The consecutive removal of glucose residues from G_2M_X glycans by glucosidase II is presented in Scheme 2. The reaction mechanism of glucosidase II is composed of three reversible reactions (reactions 1, 3, and 5) and two irreversible catalytic reactions (reactions 2 and 4). In the first reaction (reaction 1), a complex between the enzyme and G_2M_X is formed, followed by irreversible removal of the outer glucose residue and release of G_1M_X from the enzyme (reaction 2). The same order of events leads to the removal of the inner glucose (reactions 3 and 4), yielding G_0M_X. Glucosidase II can reassociate with G_0M_X to form a reversible enzyme−end product complex (reaction 5). Reaction 6 handles the reversible interaction of calnexin/calreticulin with G_1M_X. The reactions were translated into six coupled nonlinear ordinary differential equations using the standard chemical−kinetic formalism. As will be described herein, the reactions that constitute our model are required and sufficient for an accurate reconstruction of the experiments carried out by Totani et al. (*15*).

In Silico Reconstruction of the in Vitro Measurements. Totani et al. measured the activity of glucosidase II toward structurally defined synthetic glycans identical in their structures to the native *N*-glycans. To reconstruct the experimental results, we set the initial conditions, e.g., the concentrations of the enzyme and the substrates, according to the published experimental protocol and solved the differential equations numerically. The rate constants of the reactions, which we used in our simulations, were selected using the Genetic Algorithm.

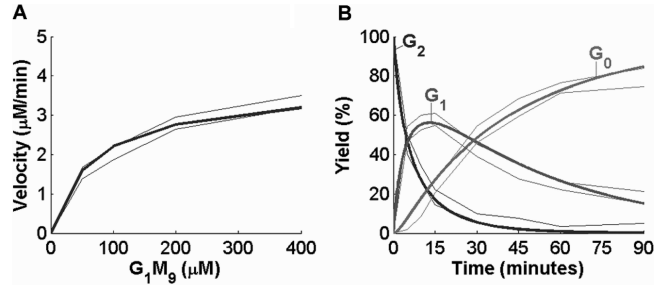

FIGURE 1: Reconstruction of the reaction of glucosidase II with M_9 glycans. (A) The initial velocity of the catalytic reaction of glucosidase II was plotted as a function of G_1M_9 concentration. (B) The graph shows the kinetics of the hydrolysis of G_2M_9 to G_1M_9 and G_0M_9. The thin lines represent the experimental data points according to their mean ± standard deviation, and the thick lines represent the reconstruction by the simulation. The graphs depict a representative solution found by the Genetic Algorithm.

Figure 1 depicts the experimental observations for M_9 glycans and the reconstructed dynamics. Panel A shows the initial velocity of the hydrolysis of G_1M_9 by glucosidase II as a function of the concentration of G_1M_9 (50−400 μM). The thin lines represent the experimental data points, and the thick line represents the reconstructed initial velocity as a function of the G_1M_9 concentration. The reconstructed line was in good agreement with the experimental data points; the velocity increased with the G_1M_9 concentration and approached the measured V_{max} value, as observed in the experiments. Panel B shows the kinetics of the hydrolysis of G_2M_9 to G_1M_9 and further to G_0M_9. The thick lines represent the reconstructed temporal concentrations of the various states of the glycan throughout the simulation, and the thin lines represent the experimental data points; the calculated lines were in good agreement with the experimental data points. The population of G_2M_9 was depleted rapidly and essentially disappeared after ∼45 min. Within this time frame, the concentration of G_1M_9 increased to a maximum (t = 15 min) and then slowly declined as the end product G_0M_9 accumulated. At t = 90 min, about 20% of the glycan still remained in the G_1M_9 state. The capacity of the simulated curve to fall within the borders of the experimental signal was impressive, but before any conclusion could be drawn, we had to evaluate the rate constants that generated the observed reconstruction.

Evaluation of the Kinetic Parameters. The kinetic parameters were determined through repeated iterations of the Genetic Algorithm. Each run of the Genetic Algorithm started with a population of 100 individuals, each having a random set of adjustable parameters that were selected within the given search range. In every generation, the individuals were evaluated by a fitness function for their ability to reconstruct the experimental results, and the best-fitting individual was reproduced. The population then underwent a series of crossovers and mutations. The worse-fitting individual of the population was replaced with the best-fitting individual. Along the progress of the runs, inferior phenotypes were gradually replaced with superior ones, eventually leading to the parameters that most accurately reconstructed the experimental observations. The parameters of the best-fitting individual after 1000 generations were defined as the solution

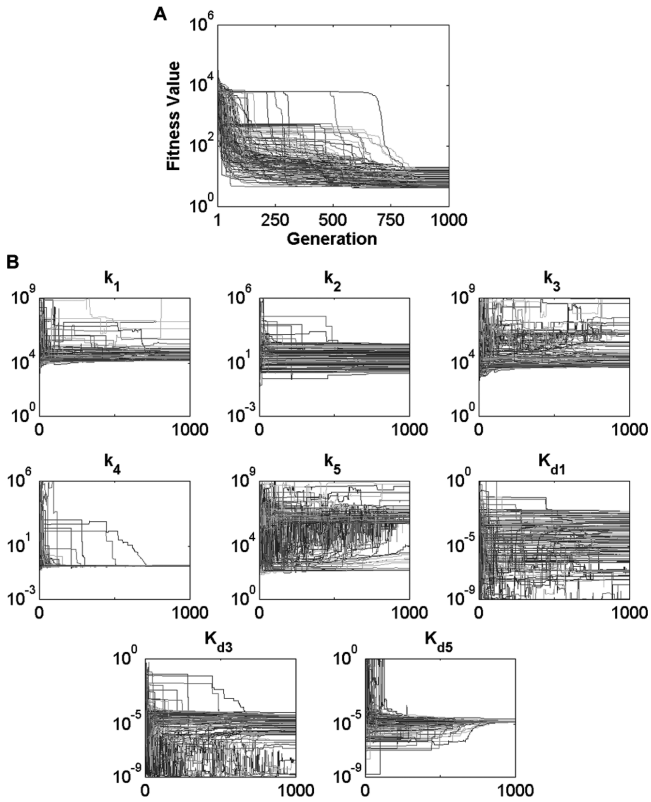

FIGURE 2: Summary of the Genetic Algorithm runs carried out to find the parameters of the reaction of glucosidase II with M_9 glycans. (A) The graph shows the variation of the fitness value of the best-fitting individual with the progress of the runs. (B) The graphs depict the variation of the adjusted parameters. The horizontal *x*-axes denote the generation number. The upper and lower scale marks of the graphs specify the search range of the parameters. Each line represents an independent run of the Genetic Algorithm.

of the run. In some cases, the simulations failed to converge to an adequate solution, i.e., within the borders of the experimental signal. These solutions were disregarded. In total, more than 100 runs reached an adequate solution. Our analysis was based only on the simulations where the reconstruction of the experimental signal fell within the boundaries of the experimental signals.

The runs of the Genetic Algorithm are summarized in Figure 2. Panel A depicts the variation of the fitness value with the progress of the runs. The fitness value, given in arbitrary units, quantifies the accuracy of the reconstruction with respect to the experimental results. The initial level was very high (approximately 5×10^4), indicating on a poor reconstruction of the experimental results, as expected for a random selection of the parameters used for the first generation. With the progress of the runs, the fitness values declined steeply, indicating that the accuracy of the reconstruction improved. Although the best solution had a fitness value of 4.06, we included in our analysis also solutions ending with higher values (up to 20.0), as their visual inspection showed them to be very close or almost identical to the best solution.

Panel B in Figure 2 presents the variation of the adjustable parameters throughout the runs. The search range of the parameters and their resulted minimal and maximal values are summarized in Table 1. Visual inspection of the frames, presented in Figure 2B, revealed that even after 1000

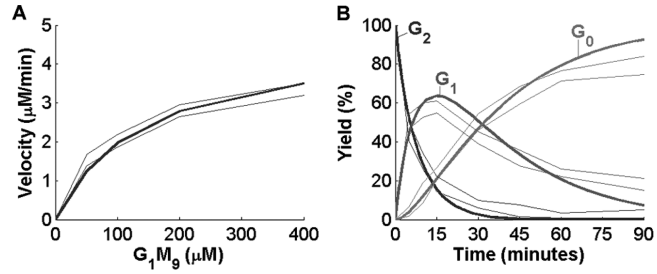

FIGURE 3: A representative solution found by the Genetic Algorithm in the absence of the interaction between glucosidase II and the end product. The system succeeded in reconstructing the initial velocity of the catalytic reaction of glucosidase II (panel A) but failed to reconstruct the kinetics of the hydrolysis of G_2M_9 to G_1M_9 and G_0M_9 (panel B).

generations, where the calculated fitness was low and constant over time, the values of most of the parameters were spread along the *y* axis except for k_4 and K_{d5} that converged to narrow ranges. The convergence of K_{d5} indicated that the interaction between glucosidase II and the nonglucosylated end product, G_0M_9, played an important role in the reaction mechanism of glucosidase II.

How can we explain the fact that some of the parameters converged to a narrow range of values while others did not converge at all? Apparently, the convergence of the parameters depended on the input of experimental observations. Once the input lacks information that is required to the convergence of the adjustable parameters, the search will fail to reach a constant value. This lack of convergence does not reflect on the validity of the model because, as shown earlier, the model accurately reconstructed the experimental observations. It should be noted that the exact values of those parameters that did not converge might be determined when additional data are available.

Interaction of Glucosidase II with G_0M_9. According to the analysis, the interaction between glucosidase II and G_0M_9 was essential for the reconstruction of the experimental observations. One advantage of the methodology we used is that we could easily modify the model (i.e., add or remove reactions) and rerun the Genetic Algorithm to test whether the modified model could reconstruct the experimental observations. Therefore, to validate our conclusion that the interaction between glucosidase II and G_0M_9 was essential, we removed reaction 5 from the overall mechanism and reran the Genetic Algorithm. We found that the system succeeded in reconstructing the dependence of the initial velocity on the concentration of G_1M_9 (Figure 3A) but failed to reconstruct the dynamics of the hydrolysis of G_2M_9 to G_1M_9 and G_0M_9 (Figure 3B). The deviation of G_2M_9 from the experimental range was rather small. Yet, at $t \geq 15$ min, the calculated disappearance of G_2M_9 was faster than the actual measured values. The deviation of G_1M_9 from the experimental range was even more profound. G_1M_9 production climbed higher and its subsequent decline was sharper than the experimental measurements. Finally, G_0M_9, the end product of the reactions, which in this scenario was not inhibitory, proceeded to completion well above the measured values. We concluded that the interaction between glucosidase II and the end product G_0M_9 is an essential part of the reaction mechanism of the enzyme.

Analysis of the Reactions between Calnexin/Calreticulin and the Glycans. The lectin chaperones calnexin and

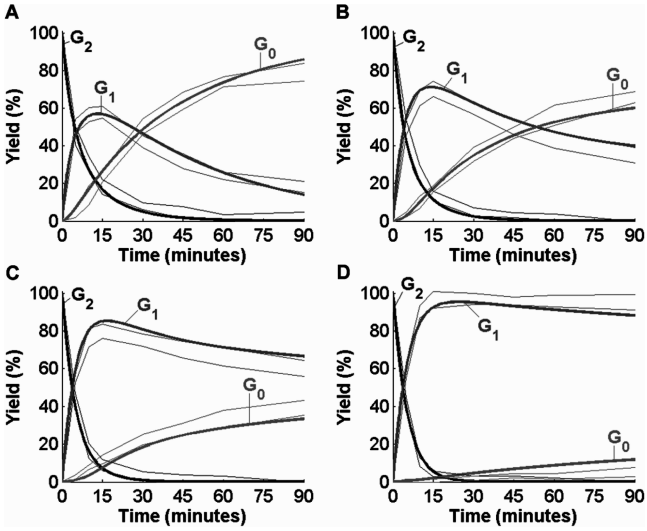

FIGURE 4: The kinetics of the reaction of glucosidase II with G_2M_9 in the presence of increasing concentrations of calreticulin. The figure depicts the kinetics of the hydrolysis of G_2M_9 to G_1M_9 and G_0M_9 in the presence of 0, 25, 50, and 75 μM calreticulin (panels A, B, C, and D, respectively). The thin lines represent the experimental data points according to their mean ± standard deviation, and the thick lines represent the reconstruction by the simulation.

calreticulin promote the folding of newly synthesized glycoproteins as part of the quality control system in the ER (*2, 27*). Although calnexin is a transmembrane protein and calreticulin is a soluble lumenal protein, sequence similarity indicates that the lectin domains of these proteins are structurally similar (*28*). The entry of the glycoproteins into the calnexin/calreticulin cycle is promoted by glucosidase II, which hydrolyzes the N-linked glycans of the glycoproteins to their monoglucosylated state. Glucosidase II also hydrolyzes the remaining glucoses of the N-linked glycans, abolishing the interaction between calnexin/calreticulin and the glycoproteins.

Totani et al. measured the hydrolysis of G_2M_9 in the presence of increasing concentrations of calreticulin (0−75 μM) (*15*). We used these measurements as an input for a *de novo* search by the Genetic Algorithm. As shown in Figure 4, the reconstructed lines agreed well with the experimental lines. Analysis of the results showed that the addition of calreticulin hardly affected the dynamics of the hydrolysis of G_2M_9 to G_1M_9. Yet, we noted that, in the higher concentrations of calreticulin, the hydrolysis of G_2M_9 was slightly faster. Apparently, calreticulin blocked G_1M_9 from interacting with glucosidase II, freeing a larger fraction of glucosidase II to hydrolyze the remaining G_2M_9. The addition of calreticulin had a remarkable effect on the hydrolysis of G_1M_9 to G_0M_9. With increasing concentrations of calreticulin, more of G_1M_9 was complexed with calreticulin, thus protected from further hydrolysis. In the higher concentration of calreticulin, most of the glycans accumulated as G_1M_9, and almost no G_0M_9 was generated (Figure 4, compare panels A, B, C, and D). A similar phenomenon was observed in another *in vitro* system, where increasing concentrations of the lumenal domain of calnexin decreased the activity of glucosidase II toward a monoglucosylated ribonuclease B (*29*).

The kinetic parameters of the reactions are summarized in Table 1 and in the Supporting Information (Figure S1). The parameters of reactions 1−5 were similar to the values calculated in the absence of calreticulin, demonstrating that our solution was consistent. Interestingly, we found that the dynamics were very sensitive to the active concentration of calreticulin. When calreticulin was assumed to be fully active, the Genetic Algorithm failed to reconstruct the experimental observations (data not shown). For this reason, the analysis included an adjustable parameter, α, reflecting the active fraction of the purified calreticulin. In all of the simulations, α converged to a constant value of $\alpha = 0.701$. We assume that, under the conditions in which the experiments were performed, the active fraction of calreticulin was approximately 70% of the total protein. The value of k_6, representing the reaction between calreticulin and G_1M_9, was found to be in the narrow range of 3.3×10^3 to 5.1×10^3 M^{-1} s^{-1}, indicating that the reaction between calreticulin and G_1M_9 was rather slow. This result is in accordance with the values reported by Patil et al. (*3*), who proposed that the slow second-order rate constant of this reaction resulted from an unfavorable activation energy of the binding of calreticulin to monoglucosylated glycans. We did not attempt to determine the dissociation constant of the calreticulin−G_1M_9 complex (K_{d6}) and used the experimental value (0.192 μM) (*4*) without any changes. The k_{off} values indicated that the half-life of the calreticulin−G_1M_9 complex was between 12 and 18 min.

It is widely accepted that glucosidase II promotes the release of the glycoproteins from calnexin and calreticulin by hydrolyzing the remaining glucose residues of the N-linked glycans (*2, 27*). This notion is corroborated by Petrescu et al. (*30*), who proposed that glucosidase II and calnexin/calreticulin approach the N-linked glycans from different sides, allowing glucosidase II to hydrolyze the N-linked glycans while the glycoproteins are bound to calnexin/calreticulin. Our simulations, which reconstructed the experimental observations, were based on the assumption that calreticulin can bind and release to and from the monoglucosylated glycans without the involvement of glucosidase II (reaction 6 in the reaction mechanism). To test whether glucosidase II actually contributes directly to the release the monoglucosylated glycans from calnexin/calreticulin, we introduced an expanded mechanism according to which glucosidase II can associate and hydrolyze the glycosidic linkage while the glycans are still bound to calnexin/calreticulin (see the text in the Supporting Information). The solution of the expanded reaction mechanism "avoided" the formation of a reactive enzyme−G_1M_9−calreticulin complex, and the contribution of this reaction to the overall flux was negligible. Hence, our results indicate that glucosidase II does not interact with the monoglucosylated glycans while the glycans are bound to calnexin/calreticulin.

Hydrolysis of the Glycans with Seven Mannose Residues by Glucosidase II. The substrate specificity of glucosidase II depends on the composition of the mannose residues in the 6′-pentamannosyl branch of the glycan (*9, 15*). To understand the basis for the specificity of the enzyme, we also analyzed the kinetic properties of M_7 glycans, for which detailed measurements were available. M_7 glycans were shown to be less reactive than M_9 glycans (*9, 15*). Figure 5 depicts the experimental observations of Totani et al. and our reconstructions. As shown in Figure 5, our model

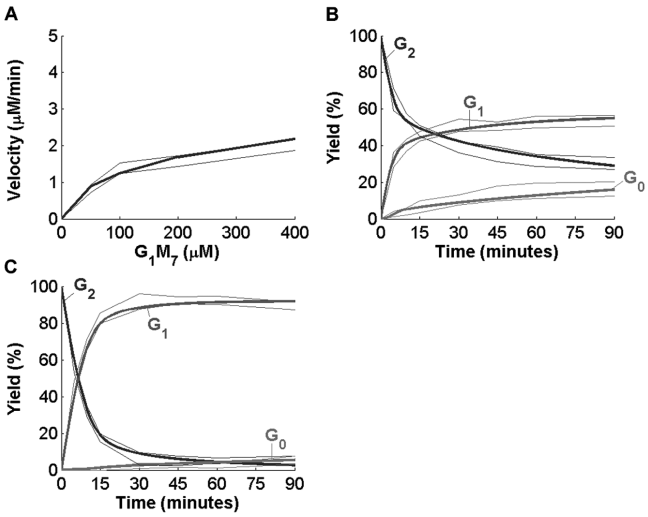

FIGURE 5: Reconstruction of the reaction of glucosidase II with M_7 glycans. (A) The initial velocity of the catalytic reaction of glucosidase II was plotted as a function of G_1M_7 concentration. (B, C) The graphs show the kinetics of the hydrolysis of G_2M_7 to G_1M_7 and G_0M_7 in the absence (B) or in the presence (C) of 75 μM calreticulin. The thin lines represent the experimental data points according to their mean $\pm$ standard deviation, and the thick lines represent the reconstruction by the simulation.

accurately reconstructed the hydrolysis of G_1M_7 to G_0M_7 (panel A) as well as the kinetics of the hydrolysis of G_2M_7 to G_1M_7 and further to G_0M_7 in the absence (panel B) and in the presence of 75 μM calreticulin (panel C). Inspection of the experimental results indicated that the initial hydrolysis of G_2M_7 to G_1M_7 was fast but declined considerably after a few minutes. Addition of 75 μM calreticulin enabled almost complete conversion of G_2M_7 to G_1M_7.

The kinetic parameters of the M_7 glycans are outlined in Table 2 and in the Supporting Information (Figure S2). The Genetic Algorithm was unable to determine the exact values of the forward rate constant of the reaction between calreticulin and G_1M_7 (k_6) and the dissociation constant of the calreticulin$-G_1M_7$ complex (K_{d6}), indicating that these reactions were not rate-limiting. An assurance for the validity of the analysis is the value of α, the active fraction of the purified calreticulin, which converged to $\alpha = 0.647 \pm 0.014$, very close to the value we obtained for M_9 glycans ($\alpha = 0.701$).

Comparison of the values obtained for the M_7 glycans and the M_9 glycans indicated that most of the kinetic parameters had similar values, except for the second catalytic rate constant (k_4) and the dissociation constant of the glucosidase II$-$end product complex (K_{d5}). In the case of the M_7 glycans, k_4 ranged between 0.2 and 0.3 s^{-1}, while in the case of the M_9 glycans, it was between 0.31 to 0.34 s^{-1}, indicating that the catalytic reaction of G_1M_7 to G_0M_7 was slightly (but significantly) slower than the reaction of G_1M_9 to G_0M_9. The value of K_{d5} for M_7 glycans was found to be lower than 0.49 μM, while for M_9 glycans it was between 15 and 23 μM, implying that glucosidase II had higher affinity to G_0M_7 than to G_0M_9.

To test the effect of k_4 on the overall dynamics, we calculated the kinetics of M_7 glycans with increasing values of k_4 (0.29, 0.34, and 0.39 s^{-1}). The aim of this experiment was to evaluate whether the low activity of glucosidase II toward the M_7 glycans was due to the low value of k_4. The

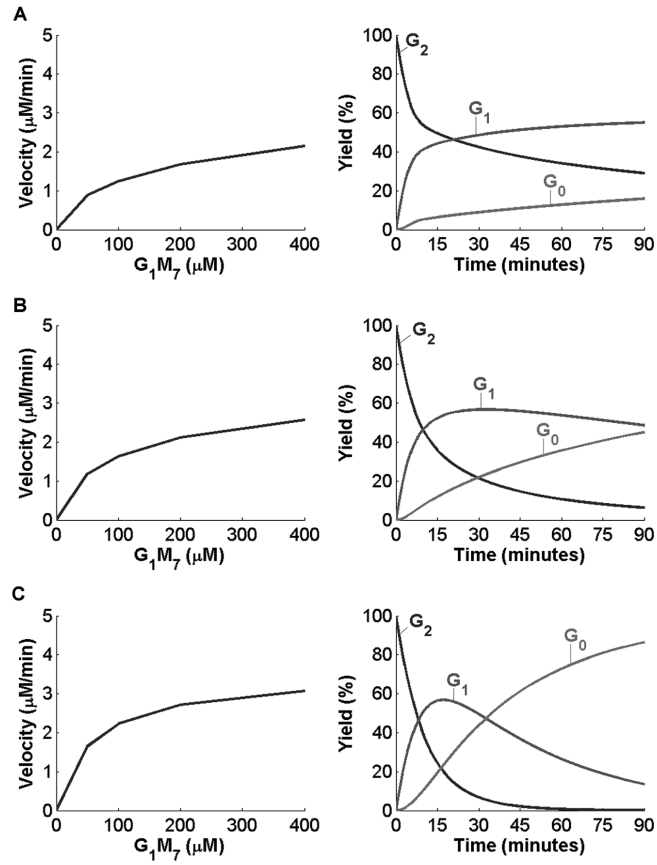

FIGURE 6: The effect of K_{d5} on the reactivity of M_7 glycans. The simulations for M_7 glycans (as in Figure 5A,B) were repeated with increasing values of K_{d5}: 0.17 μM (A), 1.7 μM (B), and 17 μM (C). The left panels show the initial velocity of the catalytic reaction of glucosidase II as a function of G_1M_7 concentration, and the right panels depict the kinetics of the hydrolysis of G_2M_7 to G_1M_7 and G_0M_7.

increase in the value of k_4 resulted in only slightly faster hydrolysis of G_1M_7 to G_0M_7 and hardly affected the hydrolysis of G_2M_7 to G_1M_7 and G_0M_7, indicating that the lower reactivity of M_7 glycans could not be the consequence of the lower value of k_4 (see the Supporting Information, Figure S3).

Next, we tested the contribution of K_{d5} to the kinetics. To this end, we repeated our calculations with increasing values of K_{d5} (0.17, 1.7, and 17 μM). As shown in Figure 6, the higher values of K_{d5} enhanced the hydrolysis of G_1M_7 to G_0M_7 (left panels) and the hydrolysis of G_2M_7 to G_1M_7 and G_0M_7 (right panels). Thus, decreasing the affinity of glucosidase II to the end product G_0M_7 resulted in much faster kinetics. Moreover, when K_{d5} was set to 17 μM (Figure 6C), which is in the range we obtained for M_9 glycans, the hydrolysis pattern of the M_7 glycans became quite similar to that of M_9 glycans. Altogether, these simulations indicated that the low activity of glucosidase II toward M_7 glycans resulted from the high affinity of the enzyme to the end product G_0M_7. We concluded that the M_9 and M_7 glycans differed from each other only with regard to the affinity of the enzyme to the end products of these glycans. On the basis of these results, we propose that the apparent low specificity of glucosidase II to the M_7 glycans, as reported by Totani et al., is the consequence of tight interaction between the enzyme and the end product G_0M_7 rather than low affinity of the enzyme to the substrate.

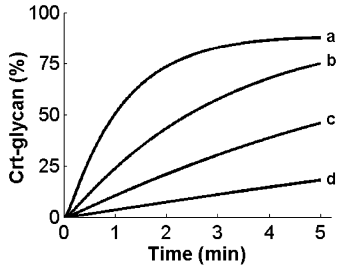

FIGURE 7: Predicting the effect of G_0M_7 on the hydrolysis of G_2M_9 to G_1M_9 and the association of the glycan with calnexin/calreticulin. Glucosidase II (1 μM) was equilibrated with G_0M_7 (0, 1, 2, and 5 μM) and then was allowed to react with 50 μM G_2M_9 in the presence of 50 μM calreticulin. The percentage of the calreticulin−glycan complex (Crt−glycan) relative to the total glycan is followed. Curves a, b, c, and d relate to the dynamics in the presence of 0, 1, 2, and 5 μM G_0M_7, respectively.

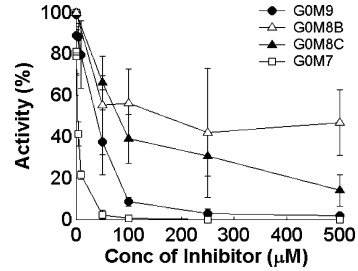

FIGURE 8: Inhibition of glucosidase II by nonglucosylated glycans. Activity for the glucosidase II-mediated glucose trimming reaction with G_2M_9 in the presence of various nonglucosylated glycans as inhibitors. The enzyme assays were carried out in a 20 μL mixture containing 50 μM G_2M_9−MTX, 0.14 microunit of soluble rat liver glucosidase II, 1 mM deoxymannojirimycin, 0.5−500 μM inhibitor, 0.05% Triton X-100, 1 mM $CaCl_2$, and 10 mM Hepes (pH 7.4) at 37 °C. After the reactions were stopped by heating at 100 °C for 1 min, the mixtures were analyzed by HPLC under the following conditions: TSK-GEL Amide-80 column (4.6 mm × 25 cm), mobile phase CH_3CN/3% AcOH−Et_3N (pH 7.3), linear gradient from 65:35 to 50:50 in 50 min, and flow rate 1.0 mL/min at 40 °C. All assays were conducted in triplicate.

We investigated the possibility that accumulation of the intermediate G_1M_7, and not the end product G_0M_7, caused inhibition of the activity of glucosidase II. To this end, we generated a new model in which the interaction between glucosidase II and G_0M_7 (reaction 5 in the original model) was replaced with a nonproductive interaction between glucosidase II and G_1M_7. We translated the new model to coupled nonlinear ordinary differential equations and used the Genetic Algorithm to fit the experimental observations, exactly as described above. As shown in the Supporting Information (Figure S4), in contrast to the original model, the new model failed to reconstruct the experimental observations. This result indicated that the inhibition of the activity of glucosidase II could not be explained by accumulation of G_1M_7, supporting our model according to which glucosidase II is inhibited by its nonglucosylated end products.

Predicting the Effect of G_0M_7 on the Entry of Newly Synthesized Glycoproteins into the Calnexin/Calreticulin Cycle. The ER contains glycoproteins with eight, seven, or even less mannose residues (*31*). Since the G_0M_7 glycan was shown to severely inhibit the activity of glucosidase II, we tested its effect on the entry of newly synthesized glycoproteins into the calnexin/calreticulin cycle. We made no attempt to model the removal of the outer glucose residue by glucosidase I, because, as stated earlier, this step occurs immediately after the binding of the core glycan to the glycoprotein. We equilibrated glucosidase II with increasing concentrations of G_0M_7 (0−5 μM) and then let the enzyme to react with G_2M_9 in the presence of calreticulin. The outcome of these simulations is depicted in Figure 7. In the absence of G_0M_7 (curve a), the glycan associated with calreticulin within 5 min as a result of the hydrolysis of the glycan to its monoglucosylated state by glucosidase II. With increasing concentrations of G_0M_7 (curves b, c, and d), the binding of calreticulin to the glycan was severely slowed as a result of the inhibition of glucosidase II by G_0M_7. Thus, even low concentrations of the G_0M_7 glycan (up to 10%) can inhibit the entry of newly synthesized glycoproteins into the calnexin/calreticulin cycle.

Inhibition of Glucosidase II by Nonglucosylated Glycans. Our kinetic analysis suggested that the interaction between glucosidase II and its nonglucosylated end products is an essential part of the reaction mechanism of the enzyme. To corroborate our prediction that these nonglucosylated end products are indeed inhibitors of glucosidase II, we measured the hydrolysis of G_2M_9 (50 μM) in the presence of nonglucosylated glycans (G_0M_9, G_0M_{8B}, G_0M_{8C}, and G_0M_7) at various concentrations (0.5−500 μM). As depicted in Figure 8, our experiments demonstrated that all of these glycans inhibited the activity of glucosidase II in a concentration-dependent manner. Moreover, we found that the G_0M_7 glycan was the strongest inhibitor, with a half-maximal inhibitory concentration (IC_{50}) of approximately 4 μM, while the IC_{50} of the G_0M_9 glycan was 10-fold higher, approximately 40 μM. The G_0M_{8C} glycan seemed to be less active, with an IC_{50} value around 100 μM. We were unable to determine the IC_{50} value of the G_0M_{8B} glycan with certainty.

DISCUSSION

In the present study, we developed a kinetic model that describes the interactions between glucosidase II, calnexin/calreticulin, and the N-linked glycans. Our model accurately reconstructed the hydrolysis of the M_9 and M_7 glycans, for which detailed measurements were available. We found that the interaction between glucosidase II and its nonglucosylated end products was essential for the reconstruction of the experimental results. Furthermore, our kinetic analysis suggested that glucosidase II had higher affinity to G_0M_7 than to G_0M_9. Other than that, we were unable to identify any considerable differences in the kinetic parameters of these glycans. It implied that the low reactivity of the M_7 glycans did not result from lower specificity of the enzyme to this glycan but from the accumulation of nonglucosylated end products in the reaction solution, imposing a general slowdown of the hydrolysis of the glycans by glucosidase II. To corroborate this idea, inhibition experiments were performed, and indeed, they demonstrated that the hydrolysis of G_2M_9 by glucosidase II was severely inhibited by the G_0M_7 glycan. These experiments are adding to the findings of Totani et al. (*15*), who showed that the hydrolysis of G_1M_9 was hindered in the presence of various nonglucosylated glycans.

Our findings suggest that glycans with a different number of mannose residues can be, at least in some cases, equivalent substrates of glucosidase II, in contrast to what had been

previously thought. It is important to note that Totani et al. (*15*) showed that the G_1M_{8B} glycan had nearly the same reactivity as G_1M_9, although the reactivity of G_1M_{8C} was much lower. In the ER, high-mannose glycans are generated by mannosidases during the maturation of the glycoproteins. Trimming of the glycoproteins defines a "window of opportunity" for the glycoproteins to fold properly, after which misfolded glycoproteins are delivered for ERAD (*11, 13*). In fact, *N*-glycans of many misfolded glycoproteins undergo extensive hydrolysis before being delivered to ERAD (*32*−*35*). Moreover, hydrolysis of mannose residues is still required for glycoprotein degradation in glycosylation-defective cell lines, carrying truncated N-linked glycans with five mannose residues instead of nine (*36*−*38*). The ability of glucosidase II to act on the M_{8B} and M_7 glycans guarantees that the folding of the glycoproteins in the calnexin/calreticulin cycle would not be delayed as a result of the trimming of the mannose residues.

The entry of newly synthesized glycoproteins into the calnexin/calreticulin cycle occurs after the sequential removal of two glucose residues from the core glycans of the glycoproteins by glucosidase I and II. Several models suggest that calnexin and calreticulin remain bound to their substrates until glucosidase II removes the remaining glucose residue. Our kinetic analysis indicates that calnexin and calreticulin can dissociate spontaneously from the monoglucosylated glycans, without any involvement of glucosidase II. This conclusion is consistent with Zapun et al. (*29*), who showed *in vitro* that the interaction between the lumenal domain of calnexin and a monoglucosylated ribonuclease B was dynamic. Furthermore, the crystal structure of the lumenal domain of calnexin implies that the glycosidic linkage is not readily accessible to glucosidase II (*39*). Thus, the role of glucosidase II is to enable the initial binding of calnexin/calreticulin to the glycoproteins and later to stop the interaction. In the meantime, calnexin and calreticulin can cycle on and off the glycoproteins freely several times. Accordingly, GT, which monitors the folding state of the glycoproteins, gets into action only in cases where additional rounds of cycling with calnexin/calreticulin are required. The mechanism presented here explains why certain glycoproteins are not affected by the deletion of UGT1, the gene coding for GT (*40, 41*), and how folding of glycoproteins can occur in *Saccharomyces cerevisiae* lacking any functional homologue of GT (*42*). In these cases, the glycoproteins complete their folding under calnexin/calreticulin in the first round of cycling, and there is no need for an extension of the folding time.

The present analysis of the observed kinetics yields rather slow dissociation kinetics of the monoglucosylated glycan from calreticulin. It should be noted that in living cells, unlike the situation in the test tube, the glycoproteins usually leave the ER once they assume their correct conformation. Therefore, the interaction time with calnexin and calreticulin should not only depend on the dissociation constants of the calnexin/calreticulin−glycan complexes but also on the folding behavior of a specific glycoprotein. In addition, the interaction time should be affected by the number of glycans on the glycoprotein (*43*). In this context, it is important to note that protein−protein interactions can also affect the kinetics. For instance, binding of calnexin and calreticulin to the glycoproteins via the polypeptide binding site can stabilize the interaction (*6*). The hydrolysis of glycoprotein-linked glycans by glucosidase II is likely to be slower compared to that of free glycans due to the bulkiness of the proteins (*9, 15*). The slower hydrolysis is balanced by the observation that crowded conditions, prevailing within the ER, enhance the hydrolysis of monoglucosylated glycans (*44*).

The most interesting question raised here is whether nonglucosylated glycans can regulate the entry of newly synthesized glycoproteins into the calnexin/calreticulin cycle. As stated above, the number of mannose residues may reflect the residence time of a certain glycoprotein in the ER. Because correctly folded glycoproteins usually leave the ER by budding vesicles, the overall steady-state level of the *N*-glycans can serve as a signal of the general folding state in the ER. Thus, in normal cells, the lumen of the ER is expected to contain mainly G_1M_9 and G_0M_9 glycans attached to glycoproteins that recently entered the ER. In contrast, in cells suffering from a folding stress, the ER is expected to contain also glycans with eight, seven, or even less mannose residues, belonging to misfolded glycoproteins that are retained in the ER. This scenario is not unrealistic, as it was shown that forcing glycoproteins to stay in the ER for rather long periods of time can increase the fraction of glycans with less than nine mannose residues, due to the activity of ER mannosidases (*33, 45*−*47*).

We showed that even relatively low concentrations of the G_0M_7 glycan can severely slow the hydrolysis of G_2M_9 to G_1M_9 and thus the association of the glycan with calnexin/calreticulin. Given the inhibitory nature of the nonglucosylated glycans, it is attractive to speculate that these end product glycans play some role in regulating the entry of newly synthesized glycoproteins into the calnexin/calreticulin cycle under folding stress conditions.

We should emphasize that our aim in this work was not to model the quality control process taking place in the ER but to further the understanding of the reaction mechanism of glucosidase II and its interaction with calnexin/calreticulin. We show that combining theory and experimentation results in a synergy that can be very productive. We hope that our work will stimulate research aimed at elucidating the role played by nonglucosylated glycans in the calnexin/calreticulin cycle.

ACKNOWLEDGMENT

We thank Dr. Kiichiro Totani (Department of Material and Life Science, Seikei University, Japan) for providing the synthetic glycans and critical reading of the manuscript and Dor Salomon (Department of Plant Sciences, Tel Aviv University, Israel) for critical reading of the manuscript.

SUPPORTING INFORMATION AVAILABLE

Summary of the Genetic Algorithm runs carried out to find the rate constants of the reaction of glucosidase II with M_9 glycans in the presence of increasing concentrations of calreticulin (Figure S1), summary of the Genetic Algorithm runs carried out to find the parameters of the reaction of glucosidase II with M_7 glycans in the presence of increasing concentrations of calreticulin (Figure S2), a series of plots depicting the effect of increasing the value of k_4 on the reactivity of M_7 glycans (Figure S3),

simulations showing that inhibition of glucosidase II by G_1M_7 cannot explain the hydrolysis of M_7 glycans (Figure S4), and evaluation of the ability of glucosidase II to interact with G_1M_X while the glycan is bound to calnexin/calreticulin. This material is available free of charge via the Internet at http://pubs.acs.org.

REFERENCES

1. Osborne, A. R., Rapoport, T. A., and van den Berg, B. (2005) Protein translocation by the Sec61/SecY channel. *Annu. Rev. Cell Dev. Biol. 21*, 529–550.
2. Ellgaard, L., and Helenius, A. (2003) Quality control in the endoplasmic reticulum. *Nat. Rev. Mol. Cell Biol. 4*, 181–191.
3. Patil, A. R., Thomas, C. J., and Surolia, A. (2000) Kinetics and the mechanism of interaction of the endoplasmic reticulum chaperone, calreticulin, with monoglucosylated ($Glc_1Man_9GlcNAc_2$) substrate. *J. Biol. Chem. 275*, 24348–24356.
4. Totani, K., Ihara, Y., Matsuo, I., Koshino, H., and Ito, Y. (2005) Synthetic substrates for an endoplasmic reticulum protein-folding sensor, UDP-glucose:glycoprotein glucosyltransferase. *Angew. Chem., Int. Ed. Engl. 44*, 7950–7954.
5. Kapoor, M., Srinivas, H., Kandiah, E., Gemma, E., Ellgaard, L., Oscarson, S., Helenius, A., and Surolia, A. (2003) Interactions of substrate with calreticulin, an endoplasmic reticulum chaperone. *J. Biol. Chem. 278*, 6194–6200.
6. Williams, D. B. (2006) Beyond lectins: the calnexin/calreticulin chaperone system of the endoplasmic reticulum. *J. Cell Sci. 119*, 615–623.
7. Parodi, A. J. (2000) Protein glucosylation and its role in protein folding. *Annu. Rev. Biochem. 69*, 69–93.
8. Helenius, A. (1994) How N-linked oligosaccharides affect glycoprotein folding in the endoplasmic reticulum. *Mol. Biol. Cell 5*, 253–265.
9. Grinna, L. S., and Robbins, P. W. (1980) Substrate specificities of rat liver microsomal glucosidases which process glycoproteins. *J. Biol. Chem. 255*, 2255–2258.
10. Sousa, M. C., Ferrero-Garcia, M. A., and Parodi, A. J. (1992) Recognition of the oligosaccharide and protein moieties of glycoproteins by the UDP-Glc:glycoprotein glucosyltransferase. *Biochemistry 31*, 97–105.
11. Helenius, A., and Aebi, M. (2001) Intracellular functions of N-linked glycans. *Science 291*, 2364–2369.
12. Moremen, K. W., and Molinari, M. (2006) N-linked glycan recognition and processing: the molecular basis of endoplasmic reticulum quality control. *Curr. Opin. Struct. Biol. 16*, 592–599.
13. Lederkremer, G. Z., and Glickman, M. H. (2005) A window of opportunity: timing protein degradation by trimming of sugars and ubiquitins. *Trends Biochem. Sci. 30*, 297–303.
14. Cabral, C. M., Liu, Y., and Sifers, R. N. (2001) Dissecting glycoprotein quality control in the secretory pathway. *Trends Biochem. Sci. 26*, 619–624.
15. Totani, K., Ihara, Y., Matsuo, I., and Ito, Y. (2006) Substrate specificity analysis of endoplasmic reticulum glucosidase II using synthetic high mannose-type glycans. *J. Biol. Chem. 281*, 31502–31508.
16. Moscovitch, D., Noivirt, O., Mezer, A., Nachliel, E., Mark, T., Gutman, M., and Fibich, G. (2004) Determination of a unique solution to parallel proton transfer reactions using the genetic algorithm. *Biophys. J. 87*, 47–57.
17. Trombetta, E. S., Simons, J. F., and Helenius, A. (1996) Endoplasmic reticulum glucosidase II is composed of a catalytic subunit, conserved from yeast to mammals, and a tightly bound noncatalytic HDEL-containing subunit. *J. Biol. Chem. 271*, 27509–27516.
18. Penny, J. E. T., and Lindfield, G. R. (1995) *Numerical methods using MATLAB*, Ellis Horwood, New York.
19. Gutman, M., and Nachliel, E. (1997) Time-resolved dynamics of proton transfer in proteinous systems. *Annu. Rev. Phys. Chem. 48*, 329–356.
20. Alonso, J. M., Santa-Cecilia, A., and Calvo, P. (1991) Glucosidase II from rat liver microsomes. Kinetic model for binding and hydrolysis. *Biochem. J. 278* (Part 3), 721–727.
21. Alonso, J. M., Santa-Cecilia, A., and Calvo, P. (1993) Effect of bromoconduritol on glucosidase II from rat liver. A new kinetic model for the binding and hydrolysis of the substrate. *Eur. J. Biochem. 215*, 37–42.
22. Pelletier, M. F., Marcil, A., Sevigny, G., Jakob, C. A., Tessier, D. C., Chevet, E., Menard, R., Bergeron, J. J., and Thomas, D. Y. (2000) The heterodimeric structure of glucosidase II is required for its activity, solubility, and localization in vivo. *Glycobiology 10*, 815–827.
23. Ito, Y., Hagihara, S., Matsuo, I., and Totani, K. (2005) Structural approaches to the study of oligosaccharides in glycoprotein quality control. *Curr. Opin. Struct. Biol. 15*, 481–489.
24. Spiro, R. G., Zhu, Q., Bhoyroo, V., and Soling, H. D. (1996) Definition of the lectin-like properties of the molecular chaperone, calreticulin, and demonstration of its copurification with endomannosidase from rat liver Golgi. *J. Biol. Chem. 271*, 11588–11594.
25. Houck, C., Joines, J., and Kay, M. A. (1995) A Genetic Algorithm for Function Optimization: A Matlab Implementation. *NCSU-IE TR* 95–09.
26. Mezer, A., Ashery, U., Gutman, M., Project, E., Bosis, E., Fibich, G., and Nachliel, E. (2006) Systematic search for the rate constants that control the exocytotic process from chromaffin cells by a genetic algorithm. *Biochim. Biophys. Acta 1763*, 345–355.
27. Hammond, C., Braakman, I., and Helenius, A. (1994) Role of N-linked oligosaccharide recognition, glucose trimming, and calnexin in glycoprotein folding and quality control. *Proc. Natl. Acad. Sci. U.S.A. 91*, 913–917.
28. Schrag, J. D., Procopio, D. O., Cygler, M., Thomas, D. Y., and Bergeron, J. J. (2003) Lectin control of protein folding and sorting in the secretory pathway. *Trends Biochem. Sci. 28*, 49–57.
29. Zapun, A., Petrescu, S. M., Rudd, P. M., Dwek, R. A., Thomas, D. Y., and Bergeron, J. J. (1997) Conformation-independent binding of monoglucosylated ribonuclease B to calnexin. *Cell 88*, 29–38.
30. Petrescu, A. J., Butters, T. D., Reinkensmeier, G., Petrescu, S., Platt, F. M., Dwek, R. A., and Wormald, M. R. (1997) The solution NMR structure of glucosylated N-glycans involved in the early stages of glycoprotein biosynthesis and folding. *EMBO J. 16*, 4302–4310.
31. Kornfeld, S., Li, E., and Tabas, I. (1978) The synthesis of complex-type oligosaccharides. II. Characterization of the processing intermediates in the synthesis of the complex oligosaccharide units of the vesicular stomatitis virus G protein. *J. Biol. Chem. 253*, 7771–7778.
32. Foulquier, F., Duvet, S., Klein, A., Mir, A. M., Chirat, F., and Cacan, R. (2004) Endoplasmic reticulum-associated degradation of glycoproteins bearing $Man_5GlcNAc_2$ and $Man_9GlcNAc_2$ species in the MI8-5 CHO cell line. *Eur. J. Biochem. 271*, 398–404.
33. Frenkel, Z., Gregory, W., Kornfeld, S., and Lederkremer, G. Z. (2003) Endoplasmic reticulum-associated degradation of mammalian glycoproteins involves sugar chain trimming to $Man6-5GlcNAc_2$. *J. Biol. Chem. 278*, 34119–34124.
34. Hosokawa, N., Tremblay, L. O., You, Z., Herscovics, A., Wada, I., and Nagata, K. (2003) Enhancement of endoplasmic reticulum (ER) degradation of misfolded Null Hong Kong alpha1-antitrypsin by human ER mannosidase I. *J. Biol. Chem. 278*, 26287–26294.
35. Kitzmuller, C., Caprini, A., Moore, S. E., Frenoy, J. P., Schwaiger, E., Kellermann, O., Ivessa, N. E., and Ermonval, M. (2003) Processing of N-linked glycans during endoplasmic-reticulum-associated degradation of a short-lived variant of ribophorin I. *Biochem. J. 376*, 687–696.
36. Ermonval, M., Kitzmuller, C., Mir, A. M., Cacan, R., and Ivessa, N. E. (2001) N-glycan structure of a short-lived variant of ribophorin I expressed in the MadIA214 glycosylation-defective cell line reveals the role of a mannosidase that is not ER mannosidase I in the process of glycoprotein degradation. *Glycobiology 11*, 565–576.
37. Olivari, S., Cali, T., Salo, K. E., Paganetti, P., Ruddock, L. W., and Molinari, M. (2006) EDEM1 regulates ER-associated degradation by accelerating de-mannosylation of folding-defective polypeptides and by inhibiting their covalent aggregation. *Biochem. Biophys. Res. Commun. 349*, 1278–1284.
38. Molinari, M. (2007) N-glycan structure dictates extension of protein folding or onset of disposal. *Nat. Chem. Biol. 3*, 313–320.
39. Schrag, J. D., Bergeron, J. J., Li, Y., Borisova, S., Hahn, M., Thomas, D. Y., and Cygler, M. (2001) The Structure of calnexin, an ER chaperone involved in quality control of protein folding. *Mol. Cell 8*, 633–644.
40. Solda, T., Galli, C., Kaufman, R. J., and Molinari, M. (2007) Substrate-specific requirements for UGT1-dependent release from calnexin. *Mol. Cell 27*, 238–249.
41. Molinari, M., Galli, C., Vanoni, O., Arnold, S. M., and Kaufman, R. J. (2005) Persistent glycoprotein misfolding activates the

glucosidase II/UGT1-driven calnexin cycle to delay aggregation and loss of folding competence. *Mol. Cell 20*, 503–512.
42. Fernandez, F. S., Trombetta, S. E., Hellman, U., and Parodi, A. J. (1994) Purification to homogeneity of UDP-glucose:glycoprotein glucosyltransferase from Schizosaccharomyces pombe and apparent absence of the enzyme for Saccharomyces cerevisiae. *J. Biol. Chem. 269*, 30701–30706.
43. Vanoni, O., Paganetti, P., and Molinari, M. (2008) Consequences of individual N-glycan deletions and of proteasomal inhibition on secretion of active BACE. *Mol. Biol. Cell* (in press).
44. Totani, K., Ihara, Y., Matsuo, I., and Ito, Y. (2008) Effects of macromolecular crowding on glycoprotein processing enzymes. *J. Am. Chem. Soc. 130*, 2101–2107.
45. Bischoff, J., Liscum, L., and Kornfeld, R. (1986) The use of 1-deoxymannojirimycin to evaluate the role of various alpha-mannosidases in oligosaccharide processing in intact cells. *J. Biol. Chem. 261*, 4766–4774.
46. Caramelo, J. J., and Parodi, A. J. (2008) Getting in and out from calnexin/calreticulin cycles. *J. Biol. Chem. 283*, 10221–10225.
47. Weng, S., and Spiro, R. G. (1993) Demonstration that a kifunensine-resistant alpha-mannosidase with a unique processing action on N-linked oligosaccharides occurs in rat liver endoplasmic reticulum and various cultured cells. *J. Biol. Chem. 268*, 25656–25663.

BI801545D